

Shelf Life Degradation of Bulk Heterojunction Solar Cells: Intrinsic Evolution of Charge Transfer Complex

Antonio Guerrero,* Hamed Heidari, Teresa S. Ripolles, Alexander Kovalenko, Martin Pfannmöller, Sara Bals, Louis-Dominique Kauffmann, Juan Bisquert, and Germà Garcia-Belmonte*

Achievement of long-term stability of organic photovoltaics is currently one of the major topics for this technology to reach maturity. Most of the techniques used to reveal degradation pathways are destructive and/or do not allow for real-time measurements in operating devices. Here, three different, nondestructive techniques able to provide real-time information, namely, film absorbance, capacitance–voltage (C–V), and impedance spectroscopy (IS), are combined over a period of 1 year using non-accelerated intrinsic degradation conditions. It is discerned between chemical modifications in the active layer, physical processes taking place in the bulk of the blend from those at the active layer/contact interfaces. In particular, it is observed that during the ageing experiment, the main source for device performance degradation is the formation of donor–acceptor charge-transfer complex (P3HT^{•+}–PCBM^{•-}) that acts as an exciton quencher. Generation of these radical species diminishes photocurrent and reduces open-circuit voltage by the creation of electronic defect states. Conclusions extracted from absorption, C–V, and IS measurements will be further supported by a range of other techniques such as atomic force microscopy, X-ray diffraction, and dark-field imaging of scanning transmission electron microscopy on ultrathin cross-sections.

1. Introduction

Research on materials and processing in organic photovoltaic (OPV) devices has led to impressive improvements over the last few years, with power conversion efficiencies (PCE) now reaching 10% for bulk heterojunction (BHJ) solar cells.^[1] In this type of devices, an interpenetrating matrix of donor and acceptor molecules harvests sun light and generates charges via photoinduced charge transfer that finally are collected at selective electrodes.^[2] Research in OPV has mainly been focused on three fronts: First, the design and synthesis of new semiconducting materials;^[2–4] second, the understanding on how the charge transfer and collection take place, and how interfacial effects limit the device efficiency;^[5,6] and, last but not least, closing the gap between laboratory achievements and industrial scale requirements.^[7] Long-term outdoor stability^[8] is one of the most challenging issues for building integrated applications with more than 20 years of durability.

In order to obtain further improvements in the stability of solar cells, a detailed understanding of the device degradation mechanisms is required.^[8] Known degradation mechanisms include: diffusion of water^[9] and molecular oxygen^[10–12] into the device, chemical degradation of interfaces^[12] and active material,^[13] interlayer and electrode diffusion,^[14] or electrode reaction with the organic materials.^[15] However, other sources of performance degradation have been relatively unexplored as the intrinsic evolution of chemical and morphological nature of active blend without intervention of external agents. In this direction, a recent study has shown that migration of polymer/fullerene molecules toward the electrodes during thermal ageing have been correlated with a loss in V_{oc} for degraded devices.^[16] Hence, one of the issues that still require intensive work is the understanding of specific mechanisms behind active layer intrinsic chemical evolution and its relationship to device performance.^[17]

Adequate chemical and physical interactions between donor and acceptor molecules are required to provide efficient charge separation. Indeed, efficient separation of carriers takes place via delocalized charge-transfer states,^[18,19] where negative polarons in fullerene moieties (PCBM^{•-}) seem to be strictly localized while positive polarons (P3HT^{•+}) are delocalized

Dr. A. Guerrero, Dr. T. S. Ripolles, Dr. A. Kovalenko,^[†]
Prof. J. Bisquert, Prof. G. Garcia-Belmonte
Photovoltaic and Optoelectronic Devices Group
Departament de Física
Universitat Jaume I
ES-12071 Castelló, Spain
E-mail: aguerrer@uji.es; garciag@uji.es

Dr. H. Heidari, Dr. M. Pfannmöller, Prof. S. Bals
EMAT, University of Antwerp
Groenenborgerlaan 171, B-2020 Antwerp, Belgium

Dr. L.-D. Kauffmann
Genes'Ink, 24 Avenue Gaston Imbert
13790 Rousset, France

Prof. J. Bisquert
Department of Chemistry
Faculty of Science
King Abdulaziz University
Jeddah 21589, Saudi Arabia

^[†]Present address: Faculty of Chemistry, Materials Research Centre,
Brno University of Technology, Purkyňova 118, 612 00 Brno,
Czech Republic

DOI: 10.1002/aenm.201401997



along a variable number of monomer units.^[20,21] Importantly, the polarizability of the charge-transfer states depends on the crystallinity of the fullerene domains.^[22] Then chemical and morphological changes at the donor–acceptor interface during device lifetime will directly affect the resulting photocurrent.

In this regard, it is already known from intentional degradation tests that formation of localized charge-transfer complexes (CTC) of P3HT^{•+} and oxidizing agents effectively reduces photocurrent.^[11] CTC is a generic term defined as an association of two or more molecules, in which a fraction of the electron charge is transferred from the donor to the acceptor in the electronic ground state. The resulting Coulomb attraction stabilizes the CTC.^[23] We can distinguish between strong CTC with full charge transfer usually called ion-radical salts, (they correspond to doping of the donor–acceptor material in terms of semiconductor physics with the formation of polaron states), and partial charge transfer of several degrees. In addition, full CTC can give rise to localized or delocalized charge (usually positive polarons or holes) that contribute to the polymer conductivity. After recognizing their importance, more attention should be then paid to the detrimental role of donor–acceptor complexes (clearly observable in the absorption spectra of the blends) and how CTC degrades the device performance.

Under such a complete scenario, it is usually not easy to discern on different degradation mechanisms in operating devices. A wide range of characterization techniques is available that can provide access to chemical and morphological variations in the device.^[24] For example, the structure and length scales of the donor–acceptor domains have been analyzed with techniques such as atomic force microscopy (AFM),^[25–27] scanning transmission electron microscopy (STEM)^[28,29] or grazing incidence X-ray diffraction (GXID).^[30] For a comprehensive review, the reader is referred to the work published by Pfanmüller et al.^[31] Alternatively, depth profile concentration of donor–acceptor blends has been obtained by using variable-angle spectroscopic ellipsometry (VASE),^[32] near-edge X-ray absorption fine structure spectroscopy (NEXAFS),^[33] neutron reflectivity,^[34] dynamic secondary ion mass spectroscopy (SIMS),^[35] etc. However, many of these techniques are destructive and/or do not allow for monitoring real-time chemical and morphology evolution of devices. Instead, optical and electrical measurements have the potential to provide real-time information on evolving devices, i.e., film absorption measurements can provide chemical^[11] and morphology information,^[36] capacitance–voltage (C–V) offers access to defect density^[37] and fullerene content at the cathode,^[38] and impedance spectroscopy (IS) to series resistance,^[39] recombination kinetics,^[6] and transport properties.^[40]

The present work is focused on the use of these nondestructive techniques (absorption, C–V, and IS) to provide real-time information about important efficiency degradation pathways that have not been studied in detail previously. Formation of donor–acceptor CTC (P3HT^{•+}–PCBM^{•-}) acting as an exciton quencher reduces the photocurrent, and also diminishes open-circuit voltage by the creation of electronic defect states. For this purpose, we will analyze the optical and electrical properties of poly(3-hexythiophene):[6,6]-phenyl-C61-butyric acid methyl ester (P3HT:PCBM) devices using nonaccelerated ageing conditions: Encapsulated devices with inverted architecture were kept in the glove box in the dark and were monitored during 1 year.

Conclusions extracted from absorption, C–V, and IS measurements are further supported by a range of other techniques such as STEM of cross-sections, external quantum efficiency (EQE), atomic force microscopy (AFM), and X-ray diffraction (XRD).

2. Results and Discussion

2.1. Shelf-Life Efficiency: *J*–*V* Analysis

In this work we aim at understanding morphology, chemical and active layer/contact interface modifications using nondestructive characterization techniques. For this purpose the evolution of device photovoltaic parameters upon shelf storage in the absence of oxygen, water, or light is monitored. This methodology is used because all these agents are known to accelerate the degradation of BHJ solar cells. Under these conditions changes in performance are exclusively caused by chemical/morphological evolution of active layer blend and its interaction with contacts. An inverted configuration composed by ITO/ZnO/P3HT:PCBM/MoO₃/Ag is chosen to minimize any degradation arising from the contacts. Devices are processed from ODCB as solvent, and they are kept in the glove box under dark conditions over a period of one year only interrupted by regular measurements.

Fresh devices prepared using ODCB are known to provide an adequate morphology after a thermal treatment of the blend that enables an efficient charge separation, transport of carriers and collection at the electrodes.^[43] Our processing conditions assure efficiencies of about 3% for fresh devices. Representative *J*–*V* curves measured under illumination and in the dark are monitored as a function of the experiment time (Figure 1). S-shape curves are not observed and leakage current remains nearly constant. These two results suggest us that contact degradation is not severe in contraposition to other long term degradation studies where contact alteration is the main cause for performance decay.^[44]

Devices showed a gradual reduction in efficiency (see Figure 2) from about 3% to 1.5% with shelf time decreasing all device parameters: The short-circuit current (J_{sc}) by about 3 mA cm⁻², the open-circuit potential (V_{oc}) by 150 mV and the fill factor (FF) by 10%. It is noticeable that all three photovoltaic parameters evolve following the same time profile. After approximately 1000 h of storage, constant values are attained. Once this initial performance decay has taken place, efficiencies remain rather constant. Indeed, Krebs et al. have tested the stability under outdoor conditions after this initial decay and shown that devices can be stable for at least another year if modules are properly encapsulated.^[45] Importantly by examining Figure 2 one can infer that the evolution of all four photovoltaic parameters follow a similar trend. This would entail that a unique degradation mechanism is affecting the overall device performance. Unfortunately the information extracted solely from the *J*–*V* curves does not allow ascertaining detrimental causes underlying performance reduction.

2.2. Optical Analysis of Fresh and Degraded Devices

In order to analyze photocurrent evolution, it is important to note that it depends on a number of factors such as optical

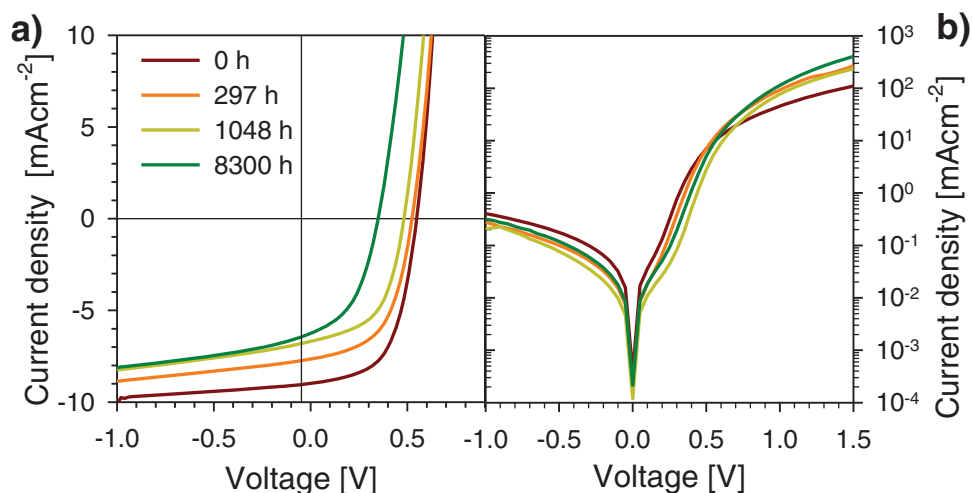


Figure 1. Representative J - V curves a) under illumination and b) in the dark as a function of the experiment time. S-shape curves are not observed and leakage current remains nearly constant both indicating that contacts do not degrade.

absorption of the active layer, charge separation, and collection. By looking specifically to the absorption spectra of the film before and after the shelf life study (Figure 3a), it is observed that the intensity of both P3HT and PCBM main peaks below 650 nm decrease moderately. Therefore, the absorption properties of the film decrease reducing the number of absorbed photons and consequently photocurrent. Quite remarkably, a

new band at 650–800 nm (≈ 1.7 eV) appears in the aged sample while the intensity in the infrared region (from 1400 to 2000 nm) slightly increases. The broad band at ≈ 900 nm does not modify the intensity being previously assigned to hole-polarons in the P3HT stabilized by ZnO.^[46] Our proposal is that this new band at 650–800 nm originates from the increment in the (P3HT^{•+}-PCBM^{•-}) CTC density (see below). It is important to highlight that the new band is not related to a scattering effect as the measurements were carried out using an integrating sphere. Additionally, the crystallinity of the P3HT does not change significantly as inferred from the relative intensity of the absorption bands of P3HT and the XRD data (see Figure S14a, Supporting Information). Accordingly, no red shift in the main absorption peak or increment of vibronic shoulder intensity are observed when comparing fresh and aged devices.

Absorption bands above 650 nm usually correlate with the P3HT^{•+} polaron formation, while the λ_{max} appears to depend on the nature of the oxidant. For example, the chemical oxidation of P3HT in the presence of oxidants such as oxygen^[47] or NOBF₄^[11] provide λ_{max} values of 760 or 710 nm, respectively. Here, in order to better understand the nature of the new absorption band exhibited by aged devices (Figure 3a), polaronic species are generated by reaction of the P3HT:PCBM films with different concentrations of the oxidant NOBF₄ as schematically drawn in Figure 3c. Corresponding absorption spectra are shown in Figure 3b. Interestingly, two polaronic bands are produced that correlate with the polaronic bands for the CTC. Absorption spectrum for low NOBF₄ concentration resembles that obtained for aged devices.

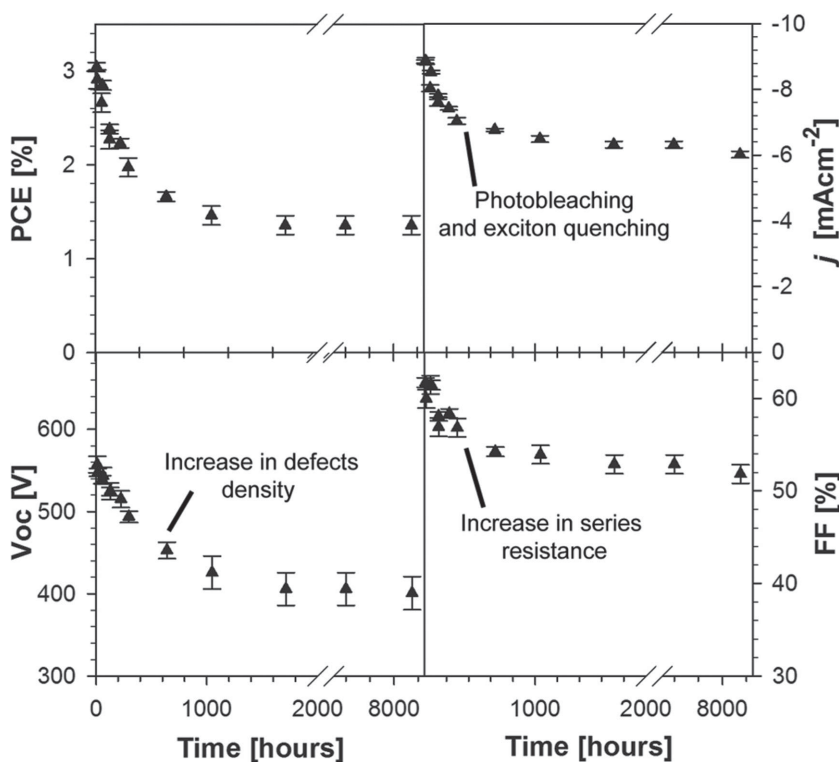


Figure 2. Device performance parameters extracted from J - V curves measured during a period of 1 year for devices fabricated with the architecture ITO/ZnO/ P3HT:PCBM/MoO₃/Ag with active layer processed from ODCB.

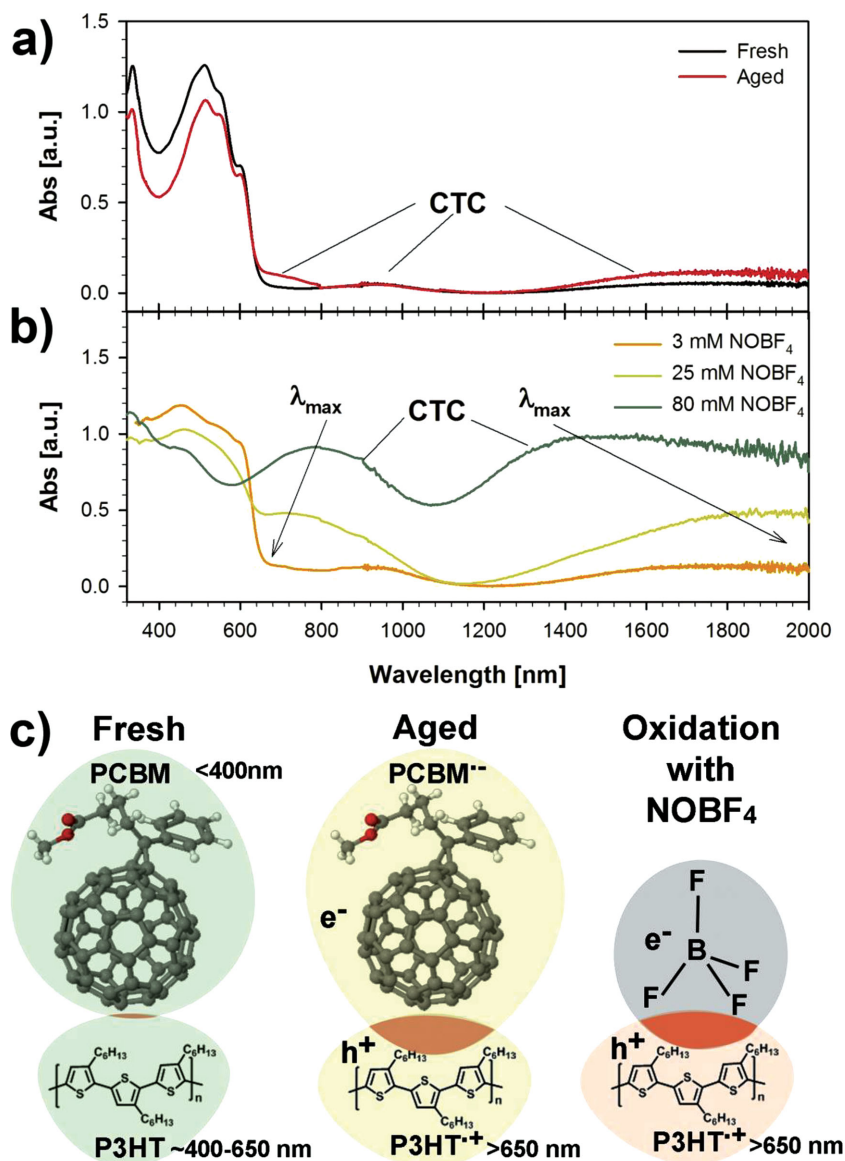


Figure 3. a) Absorption spectra of fresh and aged films cast from ODCB using integrating sphere and b) absorption of films chemically reacted with different concentrations of NOBF_4 c) Chemical structure of charge transfer complex and representative absorption bands for species present in the films for fresh and aged devices. The presence of the complex is negative for the device performance.

Their peak positions actually depend on the oxidant concentration. While λ_{max} of the high energy polaron band shifts from 800 nm at high NOBF_4 concentration (80 mM) to below 700 nm at low concentrations (3 mM), the opposite trend is observed for

To further discard the presence of oxygen, a degraded sample was thermally treated under nitrogen conditions with the intention to produce oxygen desorption as it is known to take place at temperatures of 120 °C to recover neutral P3HT

the low energy maximum with λ_{max} changing from 1450 nm to values above 2000 nm. This result clearly indicates that the properties of the actual CTC depend on the neighboring structural units. The higher concentration of polaronic species the more delocalized is the CTC as the absorption band at ≈ 700 nm is red shifted. One can therefore conclude that aging increases CTC concentration as evidenced from the similarity with polarons bands formed when external oxidant agents are used. It is important to note that formation of oxygen-related CTC is ruled out since encapsulated devices have been kept in the glove box in the absence of oxygen. Further experiments are carried out to prove the absence of oxidation reactions as next discussed.

Recently the presence of the radical anion of $\text{PCBM}^{\cdot-}$ have been detected using variable-temperature light-induced electron spin resonance in aged devices kept under static vacuum during nearly 1 month.^[21] Therefore, these considerations lead us to propose that the absorption band at 1.7 eV is related to the generation of the donor-acceptor $\text{P3HT}^{\cdot+}$ - $\text{PCBM}^{\cdot-}$ CTC, as schematically depicted in Figure 3c. Generation of such a type of species would be in agreement with the observed reduction in the intensities of neutral PCBM and P3HT peaks, which are consumed to generate the CTC. Very importantly, EQE measurements (shown in Figure S14, Supporting Information) confirm that this CTC does not contribute to the photocurrent. Integration of the absorption spectra curves predicts a decrease in the maximum current of about 10%, but the actual decrease in J_{sc} is about 35% (Table 1). Therefore, there must be other factors contributing to the reduction in photocurrent. If we then take into account that the CTC is known to be an efficient exciton quencher, then a second factor responsible for the J_{sc} decrease is found.^[48] Importantly, this band is usually not observed using accelerated degradation conditions.^[11,49]

Table 1. Photovoltaic parameters for fresh and aged devices processed under different conditions. Optical and electrical parameters extracted from J - V curves, absorption measurements and capacitance-voltage are included.

Device	J_{sc} [mA cm ⁻²]	Max $J_{\text{sc abs}}$ [mA cm ⁻²]	N [$\times 10^{16}$ cm ⁻³]	V_{oc} [mV]	Leakage current (dark - 1 V) [mA cm ⁻²]	FF [%]	PCE [%]
ODCB fresh	8.8	11.8	0.3	557	0.4	61	3.04
ODCB aged	6.0	10.6	2.3	400	0.3	51	1.30

(see Figure SI1, Supporting Information).^[50] Here, we observe that the absorption bands corresponding to neutral and the radical cation of P3HT do not change upon thermal annealing. Remarkably, temperature can be increased up to 220 °C for 3 h and the morphology of the blend do not vary as inferred from the intensity ratio of the P3HT bands. However, the intensity of the PCBM bands decreases at temperatures above 130 °C suggesting that dimerization of the PCBM molecules could have taken place.^[17,51] Interestingly, it is observed that dissolution on the active layer in ODCB does not occur as readily as it does for a freshly prepared samples annealed using the same conditions (see Figure SI1b, Supporting Information). Therefore, the presence of these radical species appears to promote partial oligomerization of the fullerene molecules locking the morphology of the active layer. This final result would explain why the solar cell performance remains almost stable after the first 1000 h.

2.3. Electrical Analysis of Fresh and Degraded Devices

As commented upon, CTC formation entails electronic alterations in the absorbing layer. The $C-V$ technique can be used to measure electrically active defects present in the organic blend of complete devices.^[37] We have previously shown that energy level equilibration at the active layer/cathode interface generates a dipole layer at the cathode contact and band bending (depletion zone) in the adjacent active layer.^[52] From analysis of the Mott–Schottky behavior defect density (N) and flat band potential (V_{fb}) can be extracted. Here, typical Mott–Schottky curves are also observed in all cases in agreement with previous reports (Figure SI2, Supporting Information).^[37] The initial and final defect density values are listed in Table 1.

Devices processed from ODCB initially show low defect levels of about $3 \times 10^{15} \text{ cm}^{-3}$ and these increase one order of magnitude after one year of shelf storage (about $2.3 \times 10^{16} \text{ cm}^{-3}$). This increase in the defect density is gradual over the whole period of study as evidenced in Figure 4a. It is noted that the defect density maximum is reached after 1000 h of storage, a time that yields almost constant photovoltaic parameter values. Therefore, there seems to be a correlation between the CTC formation and the increment in defect density measured by $C-V$, indicating that defects may indeed be originated by the presence of donor–acceptor CTC. In previous works it was shown that the intrinsic defect density correlate with the polymer crystallinity degree as measured by XRD and film absorption.^[43] However, by observing absorption spectra in Figure 3a of fresh and aged films, one can infer that the polymer structural order is unaltered after the storage period. This leads us to regard donor–acceptor CTC as the source for the defect density increase in which localized electrons in fullerene molecules act as acceptor impurities thereby enhancing the p -doping level. The proposed defect source implies the delocalization of positive polarons along a variable number of monomer units.^[20,21] CTCs have then a certain probability to create mobile holes. In fact, there is not a drastic separation between localized and delocalized CTC. Full ionization depends on the doping level and defect state energy. This would imply that a portion of CTCs are fully ionized promoting holes as quasi-free carriers, precisely

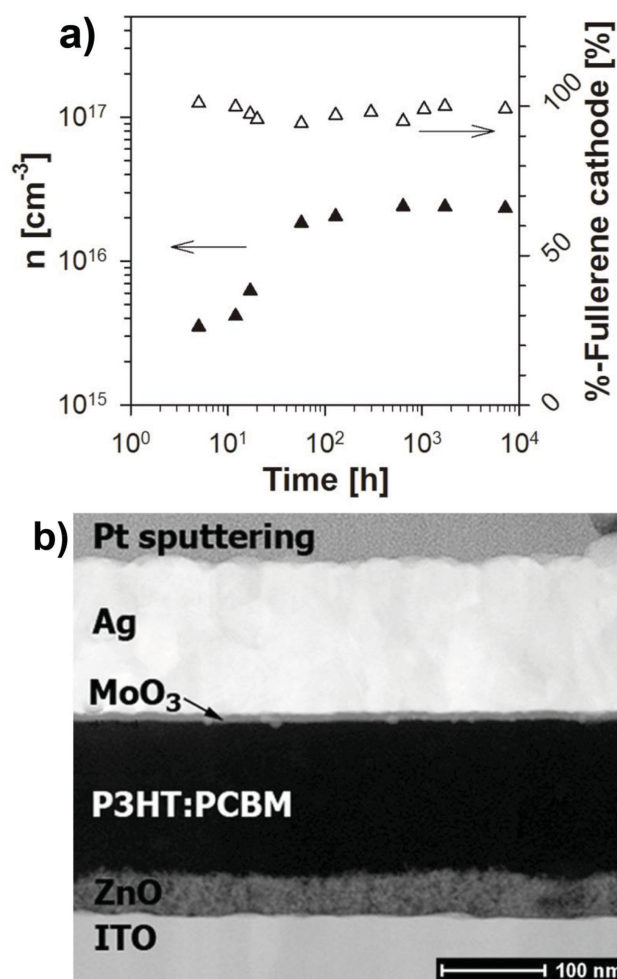


Figure 4. a) Evolution with shelf storage of defect density values (N) and calculated fullerene content at the cathode interface extracted from capacitance–voltage measurements carried out in the dark of devices cast from ODCB. b) Dark-field scanning transmission electron microscopy (STEM-DF) image of an ultrathin cross-section of a representative aged device that shows that contacts do not degrade over the lifetime.

the portion that is detected using Mott–Schottky analysis. Similar arguments were discussed in our previous work,^[11] where large reduction in the absorption band of P3HT partially correlates with the increase in the defect level resulting from Mott–Schottky analysis. This is also in good accordance with Gregg’s remarks on the charge localization degree of defect states.^[53,54]

Regarding the V_{oc} decrease, we have recently shown that defect states within the effective bandgap modulate the downshift of the hole Fermi level under illumination that in turn establishes the achievable V_{oc} .^[43] Then, it is proposed here that the observed increase in defect density is also responsible for the decrease in V_{oc} . In order to understand if this is the only factor affecting V_{oc} loss, possible contact degradation is checked as this has previously been shown to account for V_{oc} reduction during ageing of devices.^[55] Here, dark-field STEM images of cross-sections confirm that the contacts are mechanically intact after the period of one year. An image of a representative degraded device is shown in Figure 4b. A comparable image of a fresh device is provided in the Figure SI3 (Supporting

Information). In none of the cases, degradation of the inorganic layers or delamination was observed.

Relying exclusively on electrical measurements, values of flat band voltage V_{fb} can be used to detect energetic modifications in the cathode contact. This parameter may provide information on the relative coverage of the cathode contact by fullerene/polymer molecules that ultimately determine the contact selectivity. Here, we analyze the fullerene content (Figure 4a) using the method previously reported by us,^[38] observing that there is no significant variation of the degree of fullerene coverage for samples cast from ODCB. The method is fully described in the Supporting Information. AFM analysis is also included which shows no significant differences between samples (Figure SI5, Supporting Information). Additionally, we have also shown the relationship between the leakage current of the device and the fullerene content as measured from $C-V$ measurements.^[56] In the previously reported

work, high fullerene coverage of the cathode assures low leakage currents. Here leakage currents measured in the dark at -1 V during the shelf life are nearly constant (Table 1), thus indicating that aged contacts show similar selectivity than fresh devices (Figure 1b). Therefore, the decrease in V_{oc} is exclusively due to the increase in the defect density, and not to mechanisms connected to the contact degradation. This explains why V_{oc} and J_{sc} evolution with time exhibits similar trends. In both cases, there is a gradual change in the film chemistry that promotes the formation of donor-acceptor CTC (J_{sc} loss), with a concomitant defect density increase (V_{oc} reduction).

Finally, impedance spectroscopy experiments have been carried out under illumination during ageing experiments. Here, this technique is used to fully comprehend the evolution of resistive processes in devices. Impedance spectroscopy is able to discern between electrical processes taking place with different characteristic times/frequencies. In particular, recombination^[6,41] and resistive processes taking place at the contacts are observed at low frequencies,^[40,56] and transport of carriers in the high frequency region.^[39,40] Data fitting is performed using an equivalent circuit comprising two or three resistive contributions depending on whether contact effects are observable or not (see Supporting Information). Fresh samples processed with ODCB exhibit a resistive response dominated by the recombination properties with a small contribution from carrier transport. Representative spectra at different applied voltages and equivalent circuits are shown as Supporting Information (Figure SI6, Supporting Information), and a summary of the fitting results is shown in Figure 5. Series resistances derive exclusively from transport (R_{tr}) mechanisms. Recombination kinetics can be analyzed in terms of recombination resistance (R_{rec}) and chemical capacitance (C_{μ}). It is important to recall that R_{rec} is related to the recombination current derivative,^[6] therefore, high R_{rec} are desired as this represents a higher opposition of the system to lose photogenerated carriers

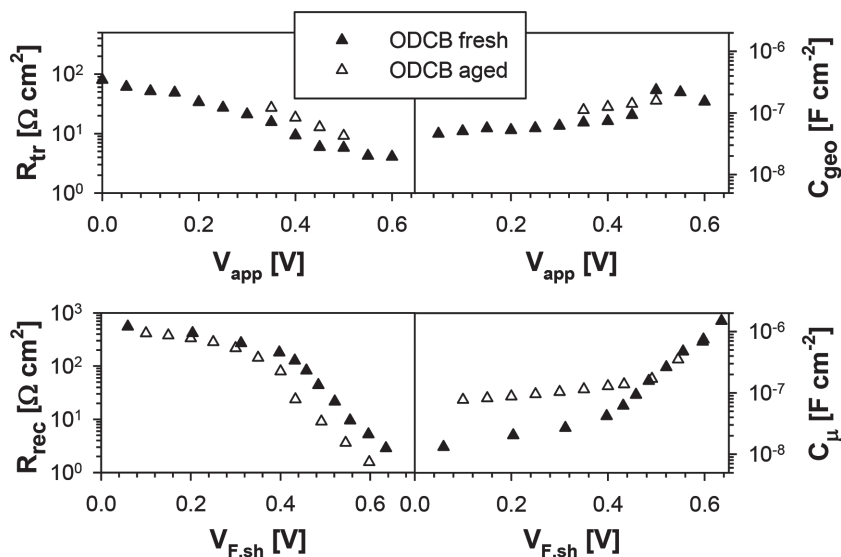


Figure 5. Fitting results extracted from impedance spectroscopy data for devices cast from ODCB. Representative devices have been measured fresh and at the end of the lifetime (aged). The equivalent circuits used are shown as supporting information.

by recombination. Here, a corrected voltage axis $V_{F,sh}$ is used to discount the voltage drop due to the series resistance with the aim of comparing devices under similar carrier densities (see Supporting Information for additional details). Interestingly, for the same $V_{F,sh}$ the extracted R_{rec} value is higher for the fresh sample indicating that the aged samples exhibit higher charge recombination. This is an extra factor limiting the V_{oc} .

Regarding electrical contributions affecting FF, there are mainly two sources: the series resistance associated to carrier transport (R_{tr}) and the voltage-dependent recombination (R_{rec}). Figure 5 shows that both R_{rec} and R_{tr} exhibit worst values in the case of aged devices.^[41] It should be stressed that devices cast from ODCB do not show extra resistances associated to contact mechanisms indicating that extraction of carriers is efficient for both fresh and aged devices, further supporting the high stability and unaltered selectivity of the contacts. Then, in ODCB-processed devices it appears that the presence of a relatively high concentration of defect states limit the ability of the system to transport efficiently charge carriers (high R_{tr}) then reducing FF.

3. Conclusions

A selection of physical techniques allows examining OPV degradation processes in real time using nondestructive methods. By analyzing the model system P3HT:PCBM processed from ODCB solvent, we show long-term performance evolution. It is feasible to distinguish between processes taking place at the outer interfaces to those occurring in the bulk of the blend. As a conclusion, the degradation is entirely related to the formation of localized donor-acceptor CTC ($P3HT^{+ \cdot}-PCBM^{- \cdot}$). Generation of CTC is responsible for photobleaching (exciton quenchers) with a concomitant increase in the density of electrically active defects. The generation of CTC species not only

diminishes photocurrent but also reduces open-circuit voltage by the creation of electronic defect states. CTC have then a detrimental effect on the overall solar cell performance. If the OPV technology truly aims to achieve long-term stability methods to avoid generation of such radical species needs to be developed.

4. Experimental Section

Solar Cell Fabrication: Devices were prepared in the inverted configuration ITO/ZnO/active layer/MoO₃/Ag. ZnO was diluted with IPA (1:1, vol:vol) and was spin coated in air at 2000 rpm for 1 min onto a precleaned ITO-coated glass substrate (10 Ohm sq⁻¹) to provide an average thickness of ≈50 nm. The substrates were heated at 100 °C for 5 min to dry the solvent and transferred to a glove box equipped with a thermal evaporator. ZnO was further thermally treated in the glove box at 130 °C for 10 min. The P3HT:PC₆₀BM solutions were cooled down to room temperature (RT) for 5 min before spin coating. Spin coating of the active layers were carried out as reported previously for P3HT:PCBM41 from *o*-dichlorobenzene (ODCB) as solvent to provide active layer thicknesses of ≈100 nm. The device fabrication was completed by thermal evaporation of 10 nm of MoO₃ and 100 nm of Ag as the anode under vacuum at a base pressure of ≈3 × 10⁻⁶ mbar. Full devices were then encapsulated with epoxy and a glass slide before testing. Samples were taken outside the glove box for *J*-*V* and *C*-*V* measurements (<15 min) and were taken back to the glove box and kept in the dark during the course of the experiment (1 year). Degradation conditions are milder than those used in ISOS-D-1 (Shelf) being the relative humidity controlled to a minimum by keeping the device in the glove box at H₂O levels below 1 ppm.^[42] To ensure that ambient exposure for short intervals of encapsulated devices did not interfere in the test, some reference devices were kept in the glove box for the whole period of study (one year period) and measured only once at the end of the test. Efficiencies of these reference devices were within the dispersion of those encapsulated devices measured several times. Some nonencapsulated devices were kept in the glove box for the whole period of the test to characterize the final state of the device using absorption and scanning transmission electron microscopy (STEM) measurements.

Film and Device Characterization: Current–density–voltage characteristics were carried out under illumination with a 1.5G source (1000 W m⁻²) using an Abet Sun 2000 Solar Simulator. The light intensity was adjusted with a calibrated Si solar cell. Capacitance–voltage and impedance spectroscopy measurements were performed using an Autolab PGSTAT-30 equipped with a frequency analyzer module. Capacitance was recorded by applying a small voltage perturbation (20 mV rms) at 1000 Hz. Measurements were carried out in the dark at several bias voltages to extract the capacitance–voltage characteristics. The optical absorption spectra of the active layers were recorded by a Cary 500 Scan VARIAN spectrophotometer in the 300–2000 nm range using an integrating sphere. Further details on materials used and other characterization techniques (XRD, AFM, STEM) are provided as Supporting Information.

Supporting Information

Supporting Information is available from the Wiley Online Library or from the author.

Acknowledgement

This work was partially supported by the FP7 European collaborative project SUNFLOWER (FP7-ICT-2011–7 Contract No. 287594), and the Generalitat Valenciana (Project No. ISIC/2012/008, Institute of Nanotechnologies for Clean Energies). S.B. acknowledges financial support from the European Research Council (ERC Starting Grant

No. 335078-COLOURATOMS). A.K. acknowledges Brno University of Technology for financial support (CZ.1.07/2.3.00/30.0039). M.P. gratefully acknowledges the SIM NanoForce program for their financial support. The authors would like to thank Dr. Beatriz Julián López for her support to carry out the absorption measurements using the integrating sphere.

Received: November 9, 2014

Published online:

- [1] M. A. Green, K. Emery, Y. Hishikawa, W. Warta, E. D. Dunlop, *Prog. Photovoltaics* **2012**, *20*, 12.
- [2] G. Yu, J. Gao, J. C. Hummelen, F. Wudl, A. J. Heeger, *Science* **1995**, *270*, 1789.
- [3] Y. Liang, Z. Xu, J. Xia, S.-T. Tsai, Y. Wu, G. Li, C. Ray, L. Yu, *Adv. Mater.* **2010**, *22*, 135.
- [4] J. Peet, J. Y. Kim, N. E. Coates, W. L. Ma, D. Moses, A. J. Heeger, G. C. Bazan, *Nat. Mater.* **2007**, *6*, 497.
- [5] A. Maurano, R. Hamilton, C. G. Shuttle, A. M. Ballantyne, J. Nelson, B. O'Regan, W. Zhang, I. McCulloch, H. Azimi, M. Morana, C. J. Brabec, J. R. Durrant, *Adv. Mater.*, **2010**, *22*, 4987.
- [6] P. P. Boix, A. Guerrero, L. F. Marchesi, G. Garcia-Belmonte, J. Bisquert, *Adv. Energy Mater.* **2011**, *1*, 1073.
- [7] F. C. Krebs, *Sol. Energy Mater. Sol. Cells* **2009**, *93*, 394.
- [8] M. Jørgensen, K. Norrman, F. C. Krebs, *Sol. Energy Mater. Sol. Cells* **2008**, *92*, 686.
- [9] K. Norrman, S. A. Gevorgyan, F. C. Krebs, *ACS Appl. Mater. Interfaces* **2009**, *1*, 102.
- [10] F. C. Krebs, S. A. Gevorgyan, J. Alstrup, *J. Mater. Chem.* **2009**, *19*, 5442.
- [11] A. Guerrero, P. P. Boix, L. F. Marchesi, T. Ripolles-Sanchis, E. C. Pereira, G. Garcia-Belmonte, *Sol. Energy Mater. Sol. Cells* **2012**, *100*, 185.
- [12] M. O. Reese, A. J. Morfa, M. S. White, N. Kopidakis, S. E. Shaheen, G. Rumbles, D. S. Ginley, *Sol. Energy Mater. Sol. Cells* **2008**, *92*, 746.
- [13] M. Manceau, A. Rivaton, J. L. Gardette, S. Guillerez, N. Lemaitre, *Polym. Degrad. Stabil.* **2009**, *94*, 898.
- [14] H. J. Kim, H. H. Lee, J. J. Kim, *Macromol. Rapid Commun.* **2009**, *30*, 1269.
- [15] C. F. Zhang, Y. Hao, S. W. Tong, Z. H. Lin, Q. A. Feng, E. T. Kang, C. X. Zhu, *IEEE Trans. Electron Devices* **2011**, *58*, 835.
- [16] I. T. Sachs-Quintana, T. Heumüller, W. R. Mateker, D. E. Orozco, R. Cheacharoen, S. Sweetnam, C. J. Brabec, M. D. McGehee, *Adv. Funct. Mater.* **2014**, *24*, 3978.
- [17] Z. Li, H. C. Wong, Z. Huang, H. Zhong, C. H. Tan, W. C. Tsoi, J. S. Kim, J. R. Durrant, J. T. Cabral, *Nat. Commun.* **2013**, *4*, 1.
- [18] A. A. Bakulin, A. Rao, V. G. Pavelyev, P. H. M. van Loosdrecht, M. S. Pshenichnikov, D. Niedzialek, J. Cornil, D. Beljonne, R. H. Friend, *Science* **2012**, *335*, 1340.
- [19] A. E. Jailaubekov, A. P. Willard, J. R. Tritsch, W.-L. Chan, N. Sai, R. Gearba, L. G. Kaake, K. J. Williams, K. Leung, P. J. Rossky, X. Y. Zhu, *Nat. Mater.* **2013**, *12*, 66.
- [20] J. Niklas, K. L. Mardis, B. P. Banks, G. M. Grooms, A. Sperlich, V. Dyakonov, S. Beaupre, M. Leclerc, T. Xu, L. Yu, O. G. Poluektov, *Phys. Chem. Chem. Phys.* **2013**, *15*, 9562.
- [21] L. Bonoldi, C. Carati, L. Montanari, R. Po', *J. Phys. Chem. C* **2014**, *118*, 7751.
- [22] B. Bernardo, D. Cheyng, B. Verreet, R. D. Schaller, B. P. Rand, N. C. Giebink, *Nat. Commun.* **2014**, *5*, 3245.
- [23] A. Y. Sosorov, D. Y. Paraschuk, *Israel J. Chem.* **2014**, *54*, 650.
- [24] W. Chen, M. P. Nikiforov, S. B. Darling, *Energy Environ. Sci.* **2012**, *5*, 8045.
- [25] B. H. Hamadani, S. Jung, P. M. Haney, L. J. Richter, N. B. Zhitenev, *Nano Lett.* **2010**, *10*, 1611.
- [26] S. Mukhopadhyay, A. J. Das, K. S. Narayan, *J. Phys. Chem. Lett.* **2012**, *4*, 161.

- [27] E. J. Spadafora, R. Demadrille, B. Ratier, B. Grévin, *Nano Lett.* **2010**, *10*, 3337.
- [28] M. Pfannmöller, H. Flügge, G. Benner, I. Wacker, C. Sommer, M. Hanselmann, S. Schmale, H. Schmidt, F. A. Hamprecht, T. Rabe, W. Kowalsky, R. R. Schröder, *Nano Lett.* **2011**, *11*, 3099.
- [29] S. S. V. Bavel, E. Sourty, G. D. With, J. Loos, *Nano Lett.* **2009**, *9*, 507.
- [30] J. Rivnay, S. C. B. Mannsfeld, C. E. Miller, A. Salleo, M. F. Toney, *Chem. Rev.* **2012**, *112*, 5488.
- [31] M. Pfannmöller, W. Kowalsky, R. R. Schröder, *Energy Environ. Sci.* **2013**, *6*, 2871.
- [32] M. Campoy-Quiles, T. Ferenczi, T. Agostinelli, P. G. Etchegoin, Y. Kim, T. D. Anthopoulos, P. N. Stavrinou, D. D. C. Bradley, J. Nelson, *Nat. Mater.* **2008**, *7*, 158.
- [33] S. Zhu, Y. Liu, M. H. Rafailovich, J. Sokolov, D. Gersappe, D. A. Winesett, H. Ade, *Nature* **1999**, *400*, 49.
- [34] D. Chen, A. Nakahara, D. Wei, D. Nordlund, T. P. Russell, *Nano Lett.* **2010**, *11*, 561.
- [35] C. M. Björström, S. Nilsson, A. Bernasik, A. Budkowski, M. Andersson, K. O. Magnusson, E. Moons, *Appl. Surf. Sci.* **2007**, *253*, 3906.
- [36] G. Li, V. Shrotriya, J. Huang, Y. Yao, T. Moriarty, K. Emery, Y. Yang, *Nat. Mater.* **2005**, *4*, 864.
- [37] P. P. Boix, G. Garcia-Belmonte, U. Munecas, M. Neophytou, C. Waldauf, R. Pacios, *Appl. Phys. Lett.* **2009**, *95*, 233302.
- [38] A. Guerrero, B. Döring, T. Ripolles-Sanchis, M. Aghamohammadi, E. Barrena, M. Campoy-Quiles, G. Garcia-Belmonte, *ACS Nano* **2013**, *7*, 4637.
- [39] A. Guerrero, T. Ripolles-Sanchis, P. P. Boix, G. Garcia-Belmonte, *Org. Electron.* **2012**, *13*, 2326.
- [40] A. Guerrero, S. Loser, G. Garcia-Belmonte, C. J. Bruns, J. Smith, H. Miyauchi, S. I. Stupp, J. Bisquert, T. J. Marks, *Phys. Chem. Chem. Phys.* **2013**, *15*, 16456.
- [41] A. Guerrero, L. F. Marchesi, P. P. Boix, J. Bisquert, G. Garcia-Belmonte, *J. Phys. Chem. Lett.* **2012**, *3*, 1386.
- [42] M. O. Reese, S. A. Gevorgyan, M. Jørgensen, E. Bundgaard, S. R. Kurtz, D. S. Ginley, D. C. Olson, M. T. Lloyd, P. Morvillo, E. A. Katz, A. Elschner, O. Haillant, T. R. Currier, V. Shrotriya, M. Hermenau, M. Riede, K. R. Kirov, G. Trimmel, T. Rath, O. Inganäs, F. Zhang, M. Andersson, K. Tvingstedt, M. Lira-Cantu, D. Laird, C. McGuinness, S. Gowrisanker, M. Pannone, M. Xiao, J. Hauch, R. Steim, D. M. DeLongchamp, R. Rösch, H. Hoppe, N. Espinosa, A. Urbina, G. Yaman-Uzunoglu, J.-B. Bonekamp, A. J. J. M. van Breemen, C. Girotto, E. Voroshazi, F. C. Krebs, *Sol. Energy Mater. Sol. Cells* **2011**, *95*, 1253.
- [43] T. S. Ripolles, A. Guerrero, G. Garcia-Belmonte, *Appl. Phys. Lett.* **2013**, *103*, 243306.
- [44] F. C. Krebs, K. Norrman, *Prog. Photovoltaics* **2007**, *15*, 697.
- [45] S. A. Gevorgyan, M. V. Madsen, H. F. Dam, M. Jørgensen, C. J. Fell, K. F. Anderson, B. C. Duck, A. Mescheloff, E. A. Katz, A. Elschner, R. Roesch, H. Hoppe, M. Hermenau, M. Riede, F. C. Krebs, *Sol. Energy Mater. Sol. Cells* **2013**, *116*, 187.
- [46] P. Ravirajan, A. M. Peiró, M. K. Nazeeruddin, M. Graetzel, D. D. C. Bradley, J. R. Durrant, J. Nelson, *J. Phys. Chem. B* **2006**, *110*, 7635.
- [47] M. S. A. Abdou, F. P. Orfino, Y. Son, S. Holdcroft, *J. Am. Chem. Soc.* **1997**, *119*, 4518.
- [48] N. Grossiord, J. M. Kroon, R. Andriessen, P. W. M. Blom, *Org. Electronics* **2012**, *13*, 432.
- [49] A. Seemann, T. Sauermann, C. Lungenschmied, O. Armbruster, S. Bauer, H. J. Egelhaaf, J. Hauch, *Sol. Energy* **2011**, *85*, 1238.
- [50] B. A. Mattis, P. C. Chang, V. Subramanian, *Synth. Met.* **2006**, *156*, 1241.
- [51] F. Piersimoni, G. Degutis, S. Bertho, K. Vandewal, D. Spoltore, T. Vangerven, J. Drijkoningen, M. K. Van Bael, A. Hardy, J. D'Haen, W. Maes, D. Vanderzande, M. Nesladek, J. Manca, *J. Polym. Sci., Part B: Polym. Phys.* **2013**, *51*, 1209.
- [52] A. Guerrero, L. F. Marchesi, P. P. Boix, S. Ruiz-Raga, T. Ripolles-Sanchis, G. Garcia-Belmonte, J. Bisquert, *ACS Nano* **2012**, *6*, 3453.
- [53] Z. Liang, A. Nardes, D. Wang, J. J. Berry, B. A. Gregg, *Chem. Mater.* **2009**, *21*, 4914.
- [54] Z. Liang, B. A. Gregg, *Adv. Mater.* **2012**, *24*, 3258.
- [55] M. T. Lloyd, D. C. Olson, P. Lu, E. Fang, D. L. Moore, M. S. White, M. O. Reese, D. S. Ginley, J. W. P. Hsu, *J. Mater. Chem.* **2009**, *19*, 7638.
- [56] A. Guerrero, N. F. Montcada, J. Ajuria, I. Etxebarria, R. Pacios, G. Garcia-Belmonte, E. Palomares, *J. Mater. Chem. A* **2013**, *1*, 12345.